French-Russian A.M.Lyapunov Institute

Preliminary report on the Project No. 99-02
01.09.2001–30.06.2002

TURBULENCE AND NOISE
IN VISCOUS COMPRESSIBLE GAS FLOWS

Project coordinators: Prof. A.Deriveux and Dr. T.Kozubskaya

Study of High Accuracy Order Schemes and Non-Reflecting Boundary Conditions for Noise Propagation Problems

Introduction

Computational aeroacoustics (CAA) problems present a great difficulty due to the necessity to consider the disturbances of different space and time scales. A way to overcome this difficulty is to use high accuracy order finite difference schemes which provide an adequate prediction of spatial-time frequency characteristics. Besides, to resolve small-scale high frequency oscillations it is needed to use fine computational meshes.

Another particularity of CAA problems consists in the fact that acoustic disturbances are completely described by the continuously-differentiated functions free from discontinuties and the solution keeps its smoothness at a linear approximation especially on fine meshes.

The above properties CAA problems' solutions require the usage of high order derivative approximations combined with the account of dispersion relations of differential hyperbolic problems under consideration.

In the case of high order schemes an accurate prescription of inflow and outflow boundary conditions for different kind of waves become very important.

In the paper a family of high order MacCormack schemes as well as the Dispersion Preserving Relation (DRP) scheme are tested on 2 problems taken from the ICASE/LaRC Workshop on Benchmark Problems in CAA. The Tam radiation and outflow conditions are used for artificial boundary treatment.

1 PROBLEM FORMULATION

1.1 General Mathematical Description

The process of propagation of small (acoustic) disturbances is simulated by the linearized Euler equations representing a linear hyperbolic equation system either with the constant coefficients or with the coefficients depending on space coordinates.

Let us consider the Euler equations for inviscid gas flows:

$$\frac{\partial Q}{\partial t} + \frac{\partial F}{\partial x} + \frac{\partial G}{\partial y} = 0,$$

where

$$Q = \begin{pmatrix} \rho \\ \rho u \\ \rho v \\ p \end{pmatrix}, \quad F = \begin{pmatrix} \rho u \\ \rho u^2 + p \\ \rho uv \\ u(E+p) \end{pmatrix}, \quad G = \begin{pmatrix} \rho v \\ \rho uv \\ \rho v^2 + p \\ v(E+p) \end{pmatrix}.$$

Then let us decompose the vector of primitive gasdynamic variables as $U' = U + \overline{U}$, $U' = (\rho\ u\ v\ p\ )^T$, $U = (\rho'\ u'\ v'\ p')^T$, $\overline{U} = (\bar\rho\ \bar u\ \bar v\ \bar p)^T$, where the parameters $\overline{U}$ present the mean flow values slowly varying (both on space and time) in relation to U:

$$\frac{\partial \bar f}{\partial t} \ll \frac{\partial f'}{\partial t}, \ \frac{\partial \bar f}{\partial x} \ll \frac{\partial f'}{\partial t}, \ \frac{\partial \bar f}{\partial y} \ll \frac{\partial f'}{\partial t}.$$

Here the flowfield $\overline{U}$ is considered known before.

If a matrix $\mathrm{P}U = Q$ of transition from primitive to conservative variables is introduced and the terms of smallness order higher than the first in relation to U are neglected one can derive the following linear equation system

$$\mathrm{P}\frac{\partial U}{\partial t} + \mathrm{A_x}\frac{\partial U}{\partial x} + \mathrm{A_y}\frac{\partial U}{\partial y} = 0,$$

or

$$\frac{\partial U}{\partial t} + \mathrm{B_x}\frac{\partial U}{\partial x} + \mathrm{B_y}\frac{\partial U}{\partial y} = 0 \tag{1}$$

$$\mathrm{B_x} = \begin{pmatrix} \bar u & \bar\rho & 0 & 0 \\ 0 & \bar u & 0 & 1/\bar\rho \\ 0 & 0 & \bar u & 0 \\ 0 & \gamma\bar p & 0 & \bar u \end{pmatrix}, \quad \mathrm{B_y} = \begin{pmatrix} \bar v & 0 & \bar\rho & 0 \\ 0 & \bar v & 0 & 0 \\ 0 & 0 & \bar v & 1/\bar\rho \\ 0 & 0 & \gamma\bar p & \bar v \end{pmatrix}.$$

All the methods given below are studied as applied to this system of linearized equations.

1.2 Benchmark Problem Formulation

A specific test case is chosen to study a set numerical algorithms intended for solving aeroacoustics problems. It is taken from the *ICASE/LaRC Workshop on Benchmark Problems in Computational Aeroacoustics (CAA)* [4].

The test problem is formulated as follows:

$$\overline{U} = \begin{pmatrix} 1.0 \\ M_x \\ M_y \\ 1/\gamma \end{pmatrix}, \; U(t=0) = \begin{pmatrix} \rho(x,y) \\ u(x,y) \\ v(x,y) \\ p(x,y) \end{pmatrix}$$

where the vector components of initial acoustic disturbances are described as

$$\begin{aligned}
\rho &= \exp(-\frac{\ln 2}{9}(x^2+y^2)) + 0.1\exp(-\frac{\ln 2}{25}((x-67)^2+Y^2)) \\
u &= 0.04Y\ \exp(-\frac{\ln 2}{25}((x-67)^2+Y^2)) \\
v &= -0.04(x-67)\ \exp(-\frac{\ln 2}{25}((x-67)^2+Y^2)) \\
p &= \exp(-\frac{\ln 2}{9}(x^2+y^2)),
\end{aligned}$$

where $Y = y$ for TEST1 problem and $Y = (y-67)$ for TEST2 problem.

This initial boundary value TEST1 problem has the following analytical solution

$$\begin{aligned}
u(x,y,t) &= \frac{x - M_x t}{2\frac{\ln 2}{25}\eta} I1 + 0.04y\ exp(-\frac{\ln 2}{25}((x-67-M_x t)^2+y^2)) \\
v(x,y,t) &= \frac{y}{2\frac{\ln 2}{9}\eta} I1 + 0.04(x-67-M_x t) exp(-\frac{\ln 2}{25}((x-67-M_x t)^2+y^2)) \\
p(x,y,t) &= \frac{1}{2\frac{\ln 2}{9}} I2 \\
\rho(x,y,t) &= p + 0.1\exp(-\frac{\ln 2}{25}((x-67-M_x t)^2+y^2))
\end{aligned} \tag{2}$$

and for TEST2 problem

$$\begin{aligned}
u(x,y,t) &= \frac{x - M_x t}{2\frac{\ln 2}{25}\eta} I1 + 0.04(y-67-M_y t) exp(-\frac{\ln 2}{25}((x-67-M_x t)^2+(y-67-M_y t)^2)) \\
v(x,y,t) &= \frac{y - M_y t}{2\frac{\ln 2}{9}\eta} I1 + 0.04(x-67-M_x t) exp(-\frac{\ln 2}{25}((x-67-M_x t)^2+(y-67-M_y t)^2)) \\
p(x,y,t) &= \frac{1}{2\frac{\ln 2}{9}} I2 \\
\rho(x,y,t) &= p + 0.1\exp(-\frac{\ln 2}{25}((x-67-M_x t)^2+(y-67-M_y t)^2))
\end{aligned} \tag{3}$$

where

$$I1(x,y,t) = \int_0^\infty \exp(-\frac{-\xi^2}{4\ln 2})\ J_1(\xi\eta)\xi \sin\xi t\, d\xi$$

$$I2(x,y,t) = \int_0^\infty \exp(-\frac{-\xi^2}{4\ln 2})\ J_0(\xi\eta)\xi \cos\xi t\, d\xi$$

$$\eta = \left((x-M_x t)^2 + (y-M_y t)^2\right)^{\frac{1}{2}}$$

J_0 and J_1 - the corresponding Bessel functions.

The following test cases are considered. In the first test problem (TEST 1) the mean flow velocities are $M_x = 0.5$, $M_y = 0.0$ which corresponds to the case of a 'horizontal wind' from the left. In the second test problem (TEST 2) these velocities are $M_x = 0.5\cos\left(\frac{\pi}{4}\right)$, $M_x = 0.5\cos\left(\frac{\pi}{4}\right)$ which corresponds to a 'diagonal wind' from the left bottom corner of a computational domain. Both problems are solved in a square $x_1 = -100, x_2 = 100, y_1 = -100, y_2 = 100$.

2 FAMILY OF MACCORMACK SCHEMES

The difference schemes constructed according to the MacCormack principle are the most dramatic examples of the 'predictor-corrector' schemes. These methods are based on the following algorithm: at the first stage a preliminary value of unknown function is calculated with the use of some difference operator ('predictor'), at the second stage this value is corrected ('corrector'), and at last a final value is calculated with the help of some procedure of averaging on 'predictor' and 'corrector' values [5, 6].

2.1 General Formulation

Let us consider the following 2D hyperbolic problem

$$\frac{\partial U}{\partial t} + \frac{\partial F}{\partial x} + \frac{\partial G}{\partial y} = 0, \tag{4}$$

where $U(x, y, t)$ – vector of unknown functions, $F(U)$ and $G(U)$ – flux vectors depending (nonlinearly, in a general case) on vector U.

As applied to the above problem, a general formulation of MacCormack methods can be presented as

$$U^*_{i,j} = U^n_{i,j} - \tau D^{(1)}_{x,i,j} F(U^n) - \tau D^{(1)}_{y,i,j} G(U^n) \tag{5}$$

$$U^{**}_{i,j} = U^*_{i,j} - \tau D^{(2)}_{x,i,j} F(U^*) - \tau D^{(2)}_{y,i,j} G(U^*) \tag{6}$$

$$U^{n+1}_{i,j} = \frac{U^n_{i,j} + U^{**}_{i,j}}{2}. \tag{7}$$

Here τ – time step, $U^n_{i,j} = U(x_i, y_j, t_n)$ – vector of unknown function in the node (x_i, y_j) at the time moment t_n, $D^{(1,2)}_{x,i,j}$, $D^{(1,2)}_{y,i,j}$ – operators of difference space derivatives on the corresponding directions. In the 'predictor' formula (5) the space derivatives $D^{(1)}_{x,i,j} F(U)$, $D^{(1)}_{y,i,j} G(U)$ are calculated in the point $U = U(x_i, y_j, t_n)$ taken from the n-th time layer, while the space derivatives $D^{(2)}_{x,i,j} F(U^*)$, $D^{(2)}_{y,i,j} G(U^*)$ in the 'corrector' formula (6) are calculated in the $U = U^*_{i,j}$ taken from (5).

Whatever the structure of operators D_x and D_y is, the above given scheme has an approximation order of $O(\tau^2)$ on time, and total approximation order of $O(\tau^2) + O(h^m)$ (hereinafter it is noted as $(2, m)$), where m – an approximation order of space derivatives by the corresponding operators.

Different realizations of this method are distinguished by the operators D_x , D_y. Here the following modifications are considered:

- classic MacCormack method $(2, 2)$
- MacCormack method $(2, 4)$
- compact MacCormack method
- compact Runge-Kutta method.

2.2 Classic MacCormack

In this method the operators of left and right difference derivatives are taken as operators $D^{(1)}_{x,i,j}$, $D^{(1)}_{y,i,j}$, and conversely the operators of right and left difference derivatives are taken as operators $D^{(2)}_{x,i,j}$, $D^{(2)}_{y,i,j}$.

$$U^*_{i,j} = U^n_{i,j} - \tau \frac{F^n_{i+1,j} - F^n_{i,j}}{\Delta x_i} - \tau \frac{G^n_{i,j+1} - G^n_{i,j}}{\Delta y_j} \tag{8}$$

$$U^{**}_{i,j} = U^*_{i,j} - \tau \frac{F^*_{i,j} - F^*_{i-1,j}}{\Delta x_{i-1}} - \tau \frac{G^*_{i,j} - G^*_{i,j-1}}{\Delta y_{j-1}} \tag{9}$$

$$U_{i,j}^{n+1} = \frac{U_{i,j}^n + U_{i,j}^{**}}{2}, \tag{10}$$

where $F_{i,j} = F(U_{i,j}^n)$, $G_{i,j} = G(U_{i,j}^n)$, $F_{i,j}^* = F(U_{i,j}^*)$, $G_{i,j}^* = G(U_{i,j}^*)$ (these notations are used from here on).

The given scheme realized on a **nonuniform** mesh is an approximation order of $(2,2)$. It can be shown by the expansion of all the terms in (8), (9) in the Taylor series in the vicinity of point (x_i, y_j).

2.3 MacCormack Schemes $(2,4)$

An approximation of space derivatives on the 5-point stencil is on the base of this method. There are a few variations of such approximation. Here the only variant from the one-parameter family of MacCormack method $(2,4)$ is presented.

$$\begin{aligned} U_{i,j}^* = U_{i,j}^n &- \frac{\tau}{\Delta x_i}\left(\alpha F_{i+2,j} + (1-2\alpha)F_{i+1,j} + (\alpha-1)F_{i,j}\right) \\ &- \frac{\tau}{\Delta y_j}\left(\alpha G_{i,j+2} + (1-2\alpha)G_{i,j+1} + (\alpha-1)G_{i,j}\right) \end{aligned} \tag{11}$$

$$\begin{aligned} U_{i,j}^{**} = U_{i,j}^* &- \frac{\tau}{\Delta x_i}\left((1-\alpha)F_{i,j}^* + (2\alpha-1)F_{i-1,j}^* - \alpha F_{i-2,j}^*\right) \\ &- \frac{\tau}{\Delta y_j}\left((1-\alpha)G_{i,j}^* + (2\alpha-1)G_{i,j-1}^* - \alpha G_{i,j-2}^*\right) \\ &- \frac{\tau}{\Delta x_j}\left(\alpha + \frac{1}{6}\right)\left(F_{i-2,j} - 2F_{i-1,j} + 2F_{i+1,j} - F_{i+2,j}\right) \\ &- \frac{\tau}{\Delta y_j}\left(\alpha + \frac{1}{6}\right)\left(G_{i,j-2} - 2G_{i,j-1} + 2G_{i,j+1} - G_{i,j+2}\right) \end{aligned} \tag{12}$$

$$U_{i,j}^{n+1} = \frac{U_{i,j}^n + U_{i,j}^{**}}{2}. \tag{13}$$

The above written 5-point one-parameter method is realized at $\alpha = 0$.

By applying the similar idea one can derive the extended formulation of algorithm (which also uses one parameter) for arbitrary non-constant rectangle mesh:

$$\begin{aligned} U_{i,j}^* = U_{i,j}^n &- \tau\left(\frac{s}{\Delta x_{i+1}}\left(F_{i+2,j} - F_{i+1,j}\right) - \frac{1-s}{\Delta x_i}\left(F_{i+1,j} - F_{i,j}\right)\right) \\ &- \tau\left(\frac{s}{\Delta y_{j+1}}\left(G_{i,j+2} - G_{i,j+1}\right) - \frac{1-s}{\Delta y_j}\left(G_{i,j+1} - G_{i,j}\right)\right) \end{aligned} \tag{14}$$

$$\begin{aligned} U_{i,j}^{**} = U_{i,j}^* &- \tau\left(\frac{1-s}{\Delta x_{i-1}}\left(F_{i,j} - F_{i-1,j}\right) - \frac{s}{\Delta x_{i-2}}\left(F_{i-1,j} - F_{i-2,j}\right)\right) \\ &- \tau\left(\frac{1-s}{\Delta y_{j-1}}\left(G_{i,j} - G_{i,j-1}\right) - \frac{s}{\Delta y_{j-2}}\left(G_{i,j-1} - G_{i,j-2}\right)\right) \end{aligned} \tag{15}$$

$$U_{i,j}^{n+1} = \frac{U_{i,j}^n + U_{i,j}^{**}}{2}. \tag{16}$$

2.4 Compact MacCormack Schemes

As applied to this method, the operators $D_{x,i,j}^{(1)}$, $D_{y,i,j}^{(1)}$ present difference operators on compact stencils [8]. Let us describe a notion of difference derivative on a compact stencil in more detail. Let it be needed to calculate a value of derivative of some function $u(x)$. And let a 3-point compact stencil is used. A theory of compact stencils is based on the supposition about the existence of dependence between the values of function u and its derivative $f = \dfrac{\partial u}{\partial x}$ in some neighboring points of computational mesh.

$$\beta_1 f_{i-1} + \beta_2 f_i + \beta_3 f_{i+1} = \alpha_1 u_{i-1} + \alpha_2 u_i + \alpha_3 u_{i+1}. \tag{17}$$

Furthermore, the coefficients $\beta_1, \beta_2, \beta_3, \alpha_1, \alpha_2, \alpha_3$ are calculated by the expansion in the Taylor series in a way to reach the accuracy needed. In doing so, in a simple case the following one-parameter family of 3-point compact stencils for an uniform mesh looks like the following:

$$\alpha_1 = -\frac{1+\alpha_2}{2h}, \alpha_3 = -\frac{1-\alpha_2}{2h}$$
$$\beta_1 = \frac{1}{6} + \frac{h\alpha_2}{4}, \beta_2 = \frac{2}{3}, \beta_3 = \frac{1}{6} - \frac{h\alpha_2}{4}$$

Here α_2 is a free parameter. The values f are calculated by solving the equation system (17) with the help of sweep algorithm. It can be shown that this method provides the accuracy of $O(h^3)$, and at $\alpha_2 = 0$ - $O(h^4)$. Here the above given method is used at $\alpha_2 = 0$.

But we can extend scheme of this algorithm up to non-constant meshes task if we assume all coefficients of derivatives to be found at the left side and all coefficients of function at the right one depending of mesh step h_i. Since in this paper we assume $h_i = x_i - x_{i-1}$, equations (17) are the following

$$\alpha_i f'_{i-1} + f'_i + \beta_i f'_{i+1} = B_i f_{i-1} + C_i f_i + A_i f_{i+1} \ , \ i = 2..N-1 \tag{18}$$

By expanding all derivatives from the left side of equation into the Teylor series of point x_i and by comparing coefficients of derivatives up to $f^{(4)}$ we obtain system of equations that defines coeficients of approximation of $O(h_i^4)$ order

$$\begin{cases} A_i \ + B_i \ + C_i & = \ 0 \\ A_i h_{i+1} - B_i h_i & = \ 1 + \alpha_i + \beta_i \\ A_i h_{i+1}^2 + B_i h_i^2 & = \ 2(\beta_i h_{i+1} - \alpha_i h_i) \\ A_i h_{i+1}^3 - B_i h_i^3 & = \ 3(\beta_i h_{i+1}^2 + \alpha_i h_i^2) \\ A_i h_{i+1}^4 + B_i h_i^4 & = \ 4(\beta_i h_{i+1}^3 - \alpha_i h_i^3) \end{cases} \tag{19}$$

This system has the unique solution

$$\begin{gathered} \alpha_i = \frac{h_{i+1}^2}{(h_{i+1}+h_i)^2} \ , \ \beta_i = \frac{h_i^2}{(h_{i+1}+h_i)^2} \ , \\ A_i = (4h_{i+1} + 2h_i)\frac{h_i^2}{h_{i+1}(h_{i+1}+h_i)^3} \ , \ B_i = -(2h_{i+1} + 4h_i)\frac{h_{i+1}^2}{h_i(h_{i+1}+h_i)^3} \ , \\ C_i = 2\frac{h_{i+1} - h_i}{h_i h_{i+1}} \ , \ i = 2..N-1 \end{gathered} \tag{20}$$

Therefore our task can be solved with $O(h_i^4)$ order of precision in inner part of computational domain. Lets pay more attention to the boundary points of equation:

$$\begin{aligned} & f'_0 + \beta_1 f'_1 = B_1 f_0 + C_1 f_1 + A_1 f_2 \ , \\ & \alpha_N f'_{N-1} + f'_N = B_N f_{N-2} + C_N f_{N-1} + A_N f_N \end{aligned} \tag{21}$$

By developing this equations as ones at the inner domain we will derive a system of equations for this coefficients. Solution of this system will give us coefficients:

$$\begin{gathered} \beta_1 = \frac{h_1 + h_2}{h_2} \ , \\ A_1 = \frac{h_1^2}{h_2^2(h_1+h_2)} \ , \ B_1 = -\frac{2h_2 + 3h_1}{h_1(h_1+h_2)} \ , \\ C_1 = \frac{(2h_2 - h_1)(h_1+h_2)}{h_2^2 h_1} \ ; \\ \alpha_N = \frac{h_{N-1} + h_N}{h_{N-1}} \ , \\ A_N = \frac{2h_{N-1} + 3h_N}{h_N(h_{N-1}+h_N)} \ , \ B_N = -\frac{h_N^2}{h_{N-1}^2(h_{N-1}+h_N)} \ , \\ C_N = \frac{(h_N - 2h_{N-1})(h_N + h_{N-1})}{h_{N-1}^2 h_N} \ ; \end{gathered}$$

One may use another configuration of boundary conditions. To do this we need to calculate a derivative at the boundary point with the aid of any computational mechanism and then assume coefficients f'_0, f_0 and f'_N, f_N at right and left sides to be equal to 1 , and assume all other coefficients to be equal to zero.

As a result we need to solve a system of N equations described by tridiagonal matrix by compact scheme to find difference derivative. One may simply realize this by sweep method

2.5 Compact Runge-Kutta Schemes

Hitherto we analysed only modifications of MacCormack method, which differ by type of difference operator of spatial derivative only. But there is no reason to avoid modification of time approximation methods. One can easy modificate it by applying Jameson procedure (which is a Runge-Kutta scheme modification) to the method constructed above [3].

3 DISPERSION RELATION PRESERVING SCHEMES

Acoustics problems are governed by the linearized Euler equations. According to wave propagation theory, the number of wave modes and their wave propagation characteristics are all encoded in the dispersion relations of the governing equations. Thus one is assured that the numerical solutions of a high order finite difference scheme will have the same number of wave modes (namely, the acoustic, vorticity, and entropy waves), the same wave propagation characteristics (namely, nondispersive, nondissipative, and isotropic) and the same wave speeds as those of the solutions of the Euler equations if both systems of equations have the same dispersion relations. Finite difference schemes which have the same dispersion relations as the original partial differential equations are referred as dispersion-relation-preserving (DRP) schemes [1].

The quality of CFD schemes is generally ranked by the order of (Taylor series) truncation. For time dependent problems, especially acoustics problems, a consistent, stable, and convergent high order scheme does not guarantee a good quality numerical wave solution. A simple analysis of the linearized compressible Euler equations reveals that in a uniform mean flow the partial differential equations support three types of waves, namely, the acoustic, the entropy, and the vorticity waves. There is no guarantee in most of the popular CFD schemes that the finite difference equations support waves with these characteristics. In fact, many current CFD codes are dispersive, anisotropic, and even highly dissipative. The main objective of this section is to present a optimized high order finite difference scheme which not only meets the usual conditions of consistency, stability, and hence convergence but also supports, in the case of small amplitude waves, wave solutions which have (as nearly as possible) the same characteristics as those of the linearized Euler equations.

It is clear that what is needed is a finite difference scheme which has the same or almost the same dispersion relation as the original partial differential equations. In a discretized system a minimum of five mesh points is needed to define a period of a sine wave. Hence the above statement needs only to be true for waves with wave numbers α, β such that $\alpha\Delta x, \beta\Delta y \leq \pi/2$ (i.e., waves with wavelengths greater than or equal to four mesh spacings), where Δx and Δy are the mesh sizes in the x and y directions, respectively.

3.1 Optimized Spatial Discretization

Consider the approximation of the first derivative $\partial f/\partial x$ at the l-th node of a uniform grid. Suppose M values of $f$to the right and N values of f to the left of this point are used to form the finite difference approximation, i.e.,

$$(\frac{\partial f}{\partial x})_l \simeq \frac{1}{\Delta x}\sum_{j=-N}^{M} a_j f_{i+j} \tag{22}$$

The usual procedure is to expand the right-hand side of (22) in Taylor series of Δx and then determine the coefficients a_j by equating coefficients of the same powers of Δx. Finite difference schemes constructed in this way will be referred to as the standard schemes. In this paper the coefficients a_j are to be chosen in a different way. It is proposed that they be determined by requiring the Fourier transform of the finite difference scheme on the right of (22) to be a close approximation of that of the partial derivative on the left.

The finite difference equation (22) is a special case of the following equation in which x is a continuous variable:

$$\frac{\partial f}{\partial x}(x) \simeq \frac{1}{\Delta x}\sum_{j=-N}^{M} a_j f(x + j\Delta x) \tag{23}$$

(22) can be recovered from (23) by setting $x = l\Delta x$. The Fourier transform and its inverse of a function are related by

$$\tilde{f}(\alpha) = \frac{1}{2\pi}\int_{-\infty}^{\infty} f(x)e^{-i\alpha x}dx \tag{24}$$

$$f(x) = \int_{-\infty}^{\infty} \tilde{f}(\alpha)e^{i\alpha x}d\alpha \tag{25}$$

The Fourier transform of the left and right sides of (23) are

$$i\alpha\tilde{f} \simeq (\frac{1}{\Delta x}\sum_{j=-N}^{M} a_j e^{i\alpha j\Delta x})\tilde{f} \tag{26}$$

By comparing the two sides of (26) it is clear that the quantity

$$\bar{\alpha} = \frac{-i}{\Delta x} \sum_{j=-N}^{M} a_j e^{i\alpha j \triangle x} \tag{27}$$

is effectively the wave number of Fourier transform of the finite difference scheme (23) or (22); $\bar{\alpha}\Delta x$ is a periodic function of $\alpha\Delta x$ with period 2π. To assure that the Fourier transform of the finite difference scheme is a good approximation of that of the partial derivative over the range of wave numbers of interest (waves with wave length longer than fourΔx or $|\alpha\Delta x| < \pi/2$) it is required that at be chosen to minimise the integrated error E defined

$$E = \int_{-\pi/2}^{\pi/2} |\alpha\Delta x - \bar{\alpha}\Delta x|^2 d(\alpha\Delta x) = \int_{-\pi/2}^{\pi/2} |ik - \sum_{j=-N}^{M} a_j e^{ijk}|^2 dk. \tag{28}$$

provides a system of linear algebraic equations by which the coefficients a_j can be easily determined. The special case of N = M is of particular interest. In this case a is real and the right-hand side of (27) is a truncated Fourier sine series. In other words, the finite difference scheme tries to approximate the partial derivative by a Fourier sine series in the wave number space. If N and M are not equal (the stencil is unsymmetric) $\bar{\alpha}$ is complex. It can be shown that when such an unsymmetric stencil is used over a large region it will generally lead to spatially growing wave solutions. To avoid this type of numerical instability, in this work, only central difference schemes will be used. Unsymmetric stencils may, however, be employed in limited regions (such as at the boundary regions of the computation domain) without leading to accumulated numerical instability. It is possible to combine the traditional truncated Taylor series finite difference approximation and the wave number For instance, if (23) be accurate to order $(\Delta x)^4$. This leaves one of the coefficients, say a,, as a fres parameter. This parameter can then be chosen to minimize the error integral E of (28). When this constrained minimization is carried out, it is straightforward to find that the coefficients are

$a_0 = 0$
$a_1 = a_{-1} = 0.79926643$
$a_2 = a_{-2} = -0.18941314$
$a_3 = a_{-3} = 0.02651995$

3.2 Optimized Time Discretization

In this paper the primary interest is on developing an explisit time marching scheme. However, the procedure formulated below may also be used to develop implicit time marching schemes.

The linearized Euler equations (22) provide the time derivatives of $\mathbf{U}$ ($\mathbf{U} = [\rho; u; v; p]^T$). Suppose the solution is known up to a time level $t = n\Delta t$. To advance to the next time step a four-level finite difference approximation in the form

$$\mathbf{U}^{(n+1)} - \mathbf{U}^{(n)} \simeq \Delta t \sum_{j=0}^{3} b_j (\frac{d\mathbf{U}}{dt})^{(n-j)} \tag{29}$$

is proposed. To ensure that the system is consistent, three of four coefficient $b_j (j = 1, 2, 3)$ will be chosen so that (29) is satisfied to order $(\Delta t)^3$ when both sides are expanded to Taylor series. This leaves one free parameter b_0. The relations between the other coefficient and b_0 are

$$b_1 = -3b_0 + 53/12;\ b_2 = b_0 - 16/3;\ b_3 = -b_0 + 23/12 \tag{30}$$

The remaining coefficients b_0 will now be determined by requiring that the Laplace transform of the above finite scheme (29) be a good approximation of that of the partial derivative.

The finite differential equation (29) is special case of the difference equation in which t is a continuous variable

$$\mathbf{U}(t + \Delta t) - \mathbf{U}(t) \simeq \Delta t \sum_{j=0}^{3} b_j \frac{d}{dt} \mathbf{U}(t - j\Delta t) \tag{31}$$

(31) is identical to (29) if t is set equal to $n\Delta t$. It will be assumed for the time being that U satisfies the following initial condition, i.e.

$$\mathbf{U}(t) = 0, t < \Delta t \tag{32}$$

By applying the Laplace transform to (31) it is easy to obtain

$$-i \frac{i(e^{-i\omega\Delta t} - 1)}{\Delta t \sum_{j=0}^{3} b_j e^{ij\omega\Delta t}} \tilde{\mathbf{U}} \simeq \frac{\widetilde{d(\mathbf{U})}}{dt} \tag{33}$$

where $\sim$ represents the Laplace transform. The Laplace transform of the time derivative of $\mathbf{U}$, i.e. the right side of (33) is, however, equal to $-i\omega\tilde{\mathbf{U}}$. Thus by comparing the two sides of (33) the quantity

$$\bar{\omega} = \frac{i(e^{-i\omega\Delta t} - 1)}{\Delta t \sum_{j=0}^{3} b_j e^{ij\omega\Delta t}} \tag{34}$$

is the effective angular frequency of the time discretization scheme (29). The weighted Integral error,E_1, incurred by using ditto approximate co will be defined by using $\bar{\omega}$ to approximate ω will be defined by

$$E_1 = \int_{-0.5}^{0.5} (\sigma[Re(\bar{\omega}\Delta t)]^2 + (1-\sigma)[Im(\bar{\omega}\Delta t - \omega\Delta t)]^2) d(\omega\Delta t) \tag{35}$$

where σ is the weight on the real part. The value b_0 is chosen to minimize E_1. It is the root of the equation

$$\frac{dE_1}{db_0} = 0 \tag{36}$$

As an example, if a weight $\sigma = 0.36$ is used (36) gives $b_0 = 2.30255809$. From (30) the other coefficients are

$$b_1 = -2.49100760;\ b_2 = 1.57434093;\ b_3 = -0.38589142 \tag{37}$$

The weight σ allows one to adjust the degree of emphasis one wishes to impose on the optimization process in favor of having better wave propagation characteristics (real part of ω) or damping characteristics (imaginary part of ω). The value $\sigma = 0.36$ appears to be a well-balanced choice.

The relationship between $\bar{\omega}$ and ω is not one to one. This means that the finite difference marching scheme (29) will contain spurious numerical solutions. It is easy to see that for a given $\bar{\omega}\Delta t$ there are four values of $\omega\Delta t$ which satisfy (34). For negative values of $\bar{\omega}$ the values of ω may be found by the extension formula

$$\omega(-\bar{\omega}) = -\omega^*(\bar{\omega}) \tag{38}$$

(* indicates the complex conjugate) which is implicit in (34). It is to be noted that three of the roots have negative imaginary parts over the entire range of $\bar{\omega}\Delta t$ shown. The fourth root has negative imaginary part only for $\bar{\omega}\Delta t$ ¡ 0.4. For larger values of $\bar{\omega}\Delta t$ the imaginary part of this root becomes positive. This spurious root could cause numerical instability if too large time step is used.

A closer examination reveals that only the root with nearly zero imaginary part gives a good approximation to the desired straightline relation $\bar{\omega} = \omega$ over a limited range of $\bar{\omega}\Delta t$ ($\bar{\omega}\Delta t$¡ 0.6; note the optimized range in (35)has accordingly been chosen to be from -0,5 to 0.5). To ensure that the dispersion relation of the wave modes supported by the finite difference scheme are close approximations of the corresponding wave modes of the Euler equations, the values of $\bar{\omega}\Delta t$ in the entire computation must be restricted at the range of -0.6 to 0.6.

4 NON-REFLECTING BOUNDARY CONDITIONS

Methods described below had been used to solve real test task, which required appropriate boundary conditions for adequate numerical solution.

Due to some motives after consideration of possible alternatives classical non-reflecting Tamm boundary conditions (*Christopher K.W.Tam*)[2] were chosen.

Radiation boundary conditions at the inflow boundary (of 2-dimensional domain) are given by

$$\left(\frac{1}{V(\theta)}\frac{\partial}{\partial t} + \frac{\partial}{\partial r} + \frac{1}{2r}\right)\begin{bmatrix}\rho\\ u\\ v\\ p\end{bmatrix} = 0 \tag{39}$$

In cartesian this system of equations becomes

$$\begin{cases} \dfrac{1}{V(\theta)}\dfrac{\partial\rho}{\partial t} + \cos\theta\,\dfrac{\partial\rho}{\partial r} + \sin\theta\,\dfrac{\rho}{2r} = 0 \\ \dfrac{1}{V(\theta)}\dfrac{\partial u}{\partial t} + \cos\theta\,\dfrac{\partial u}{\partial r} + \sin\theta\,\dfrac{u}{2r} = 0 \\ \dfrac{1}{V(\theta)}\dfrac{\partial v}{\partial t} + \cos\theta\,\dfrac{\partial v}{\partial r} + \sin\theta\,\dfrac{v}{2r} = 0 \\ \dfrac{1}{V(\theta)}\dfrac{\partial p}{\partial t} + \cos\theta\,\dfrac{\partial p}{\partial r} + \sin\theta\,\dfrac{p}{2r} = 0 \end{cases} \tag{40}$$

Boundary conditions at the outflow boundary are given by

$$\begin{cases} \dfrac{\partial \rho}{\partial t} + u_0 \dfrac{\partial \rho}{\partial x} + v_0 \dfrac{\partial \rho}{\partial y} = \dfrac{1}{a_0^2} \left(\dfrac{\partial p}{\partial t} + u_0 \dfrac{\partial p}{\partial x} + v_0 \dfrac{\partial p}{\partial y} \right) \\ \dfrac{\partial u}{\partial t} + u_0 \dfrac{\partial u}{\partial x} + v_0 \dfrac{\partial u}{\partial y} = \dfrac{1}{\rho_0} \dfrac{\partial p}{\partial x} \\ \dfrac{\partial v}{\partial t} + u_0 \dfrac{\partial v}{\partial x} + v_0 \dfrac{\partial v}{\partial y} = \dfrac{1}{\rho_0} \dfrac{\partial p}{\partial y} \\ \dfrac{1}{V(\theta)} \dfrac{\partial p}{\partial t} + \cos\theta \dfrac{\partial p}{\partial r} + \sin\theta \dfrac{p}{2r} = 0 \end{cases} \tag{41}$$

where $V(\theta) = a_0 \left(M\cos(\theta - \varphi) + \left(1 - M^2 \sin^2(\theta - \varphi)\right)^{\frac{1}{2}} \right)$, $M = \dfrac{(u_0^2 + v_0^2)^{\frac{1}{2}}}{a_0}$ and $a_0 = (\gamma p_0/\rho_0)^{\frac{1}{2}}$ is the speed of sound.

5 NUMERICAL RESULTS

All the methods described above have been tested on the test problems 1 and 2 (see Section 1.2).

5.1 Methods for rectangular meshes

The both test problems are solved on a uniform mesh of size $200 * 200$ and $100 * 100$ with Kurant number 0.1 for DRP scheme and 0.3 for MacCormack schemes and compact Runge-Kutta scheme.
Let us define the following mesh norm used below:

$$||u||_{L_2} = \left(\sum_{i=0}^{N_x} \sum_{j=0}^{N_y} |\rho - \rho^{exact}|^2 \, \Delta x_i \Delta y_j \right)^{1/2} \tag{42}$$

The Tables 1 and 2 present the errors in the calculation of density in whole area at the time moments 40 and 80 correspondingly in the norm L_2 for TEST 1.
In Table 5 shown time requirements on one time step for each method for TEST 1 and 200×200 grid.
Table 1. Density error in norm L_2 at time moment 40 (TEST 1).

Mesh	MacCormack(2,2)	MacCormack(2,4)	Compact MacCormack	Compact Runge-Kutta	DRP
100×100	2.9291963	1.2172034	0.6313619	0.7131858	0.4739973
200×200	1.5741711	0.1896858	0.1920354	0.0578551	0.0981934

Table 2. Density error in norm L_2 at time moment 80 (TEST 1).

Mesh	MacCormack(2,2)	MacCormack(2,4)	Compact MacCormack	Compact Runge-Kutta	DRP
100×100	3.0236523	1.3625812	0.8102355	0.8805833	0.5918264
200×200	1.9436269	0.2524185	0.2161615	0.0811014	0.1393590

Table 3. Density error in norm L_2 at time moment 60 (TEST 2).

Mesh	MacCormack(2,2)	MacCormack(2,4)	Compact MacCormack	CRK	DRP
time $60(200 \times 200)$	1.9706537	0.2731957	0.2918258	0.0859193	0.1468675

Table 4. Density error in norm L_2 at time moment 80 (TEST 2).

Mesh	MacCormack(2,2)	MacCormack(2,4)	Compact MacCormack	CRK	DRP
time $80(200 \times 200)$	1.9355271	0.2432919	0.2746325	0.0649704	0.1089294

Table 5. Methods resource requirements (TEST 1, 200×200).

Measure	MacCormack(2,2)	MacCormack(2,4)	Compact MacCormack	CRK	DRP
t_{method}/t_{MC22}	1.0000	1.3264	6.1170	10.4804	5.9454

As it is seen from the above Tables the most accuracy is provided by the compact Runge-Kutta scheme and DRP scheme, but when using the best compact Runge-Kutta scheme one step calculation is found two times more expansive than both the compact NacCormack and DRP schemes.

6 CONCLUSION

A general conclusion is that the solutions computed by compact MacCormack schemes (both variants under consideration) and DRP scheme agree very favorably with the exact solutions. These schemes combined with the Tam non-reflecting boundary conditions provide an accurate solution of a wide range of computational aeroacoustics problems.

If analyzing in more detail one can see that in the case of using more coarse meshes the DRP schemes produce the most accurate solutions in comparison with the ones obtained by the means of compact MacCormack schemes. When the fine meshes are used the best results are provided by the MacCormack schemes on compact stencils.

The MacCormack schemes are found less sensitive to the choice of time step which offers the production of more accurate results at the same computer costs (or less expensive results at the same accuracy) in relation with the DRP schemes.

The Tam radiation and outflow boundary conditions confirms their high quality and show a good compatibility with MacCormack and DRP schemes. Such boundary treatment allows for getting adequate results both at input and output boundaries.

The MacCormack schemes (2-2) demonstrate less accuracy and noticeable parasitic oscillations (especially at using coarse meshes) caused by their non-monotony. The same can be also related to the MacCormack (2-4) schemes (but at less extension). From this standpoint MacCormack (2-6) schemes look better but they are not convenient due to a very large stencil in use. At the same time, the non-reflecting boundary conditions appear easier and better applicable for this group of MacCormack schemes in comparison with compact MacCormack schemes.

An important note is that the DRP scheme used here is applicable only at uniform grids, and its modification for non-uniform grids is a subject of further investigations.

References

[1] **Christopher K. W. Tam, Jay C. Webb** "Dispersion-Relation-Preserving Finite Difference Schemes for Computational Acoustics", Journal of Computational Physics, volume 107, 1993.

[2] **K.W.Tam, Jun Fang, Konstatin A. Kurbatskii** "Non-homogeneous radiation and outflow boundary conditions simulating incoming acoustic and vorticity waves for exterior computational aeroacoustics problems", International Journal for Numerical Methoda in Fluids, volume 26, 1107-1123, 1998.

[3] **A. Jameson** "Numerical Solution for The Euler Equation or Compressible Inviscouse Fluid", Numerical Methods for The Euler Equations of Fluid Dynamics, 199-231, 1988.

[4] "ICASE/LaRC Workshop on Benchmark Problems in Computational Aeroacoustics(CAA)", NASA Comference Publication, Hampton, Virginia, October 24-26, 1994.

[5] **David Gottlieb, Eli Turkel** "Disipative two-four methods for time - dependent problems", Mathematics of Computation, volume 30, number 136, october 1976.

[6] **L.Gammet, F.Ducros, F.Nicoud, T.Poinsot** "Compact finite difference schemes on non-uniform meshes.Application to direct numerical simulations of compressible flows", International journal for numerical methods in fluids, volume 29, 1999.

[7] **R.Hixon** "Prefactored small-stencil compact schemes", Journal of Computational Physics, volume 165, 2000.

[8] **Tolstykh A.N.** "Compact stencils", 1988.

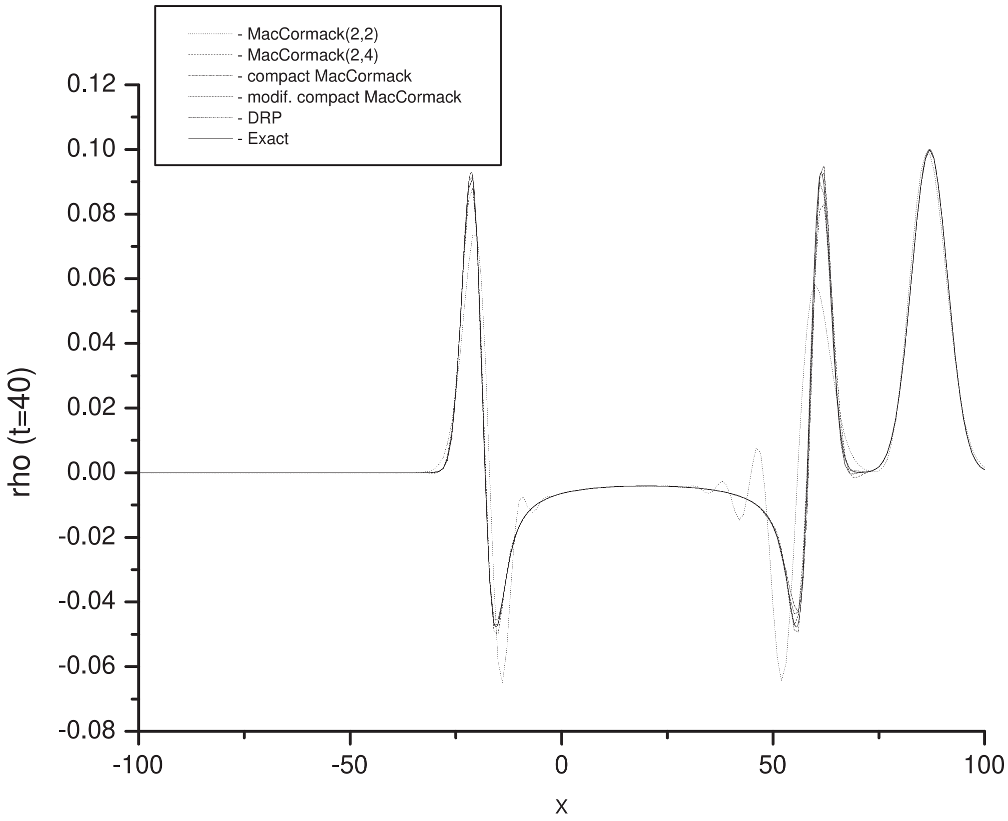

Figure 1: Density section (y=0, time 40)

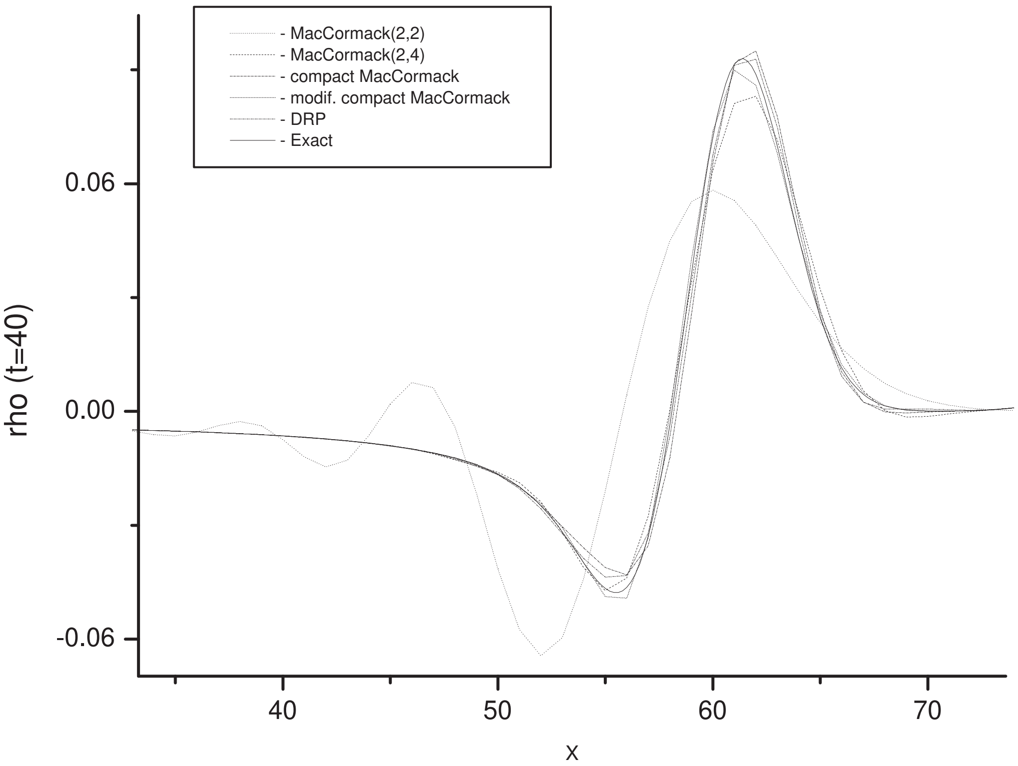

Figure 2: Density section (y=0, time 40, zoom)

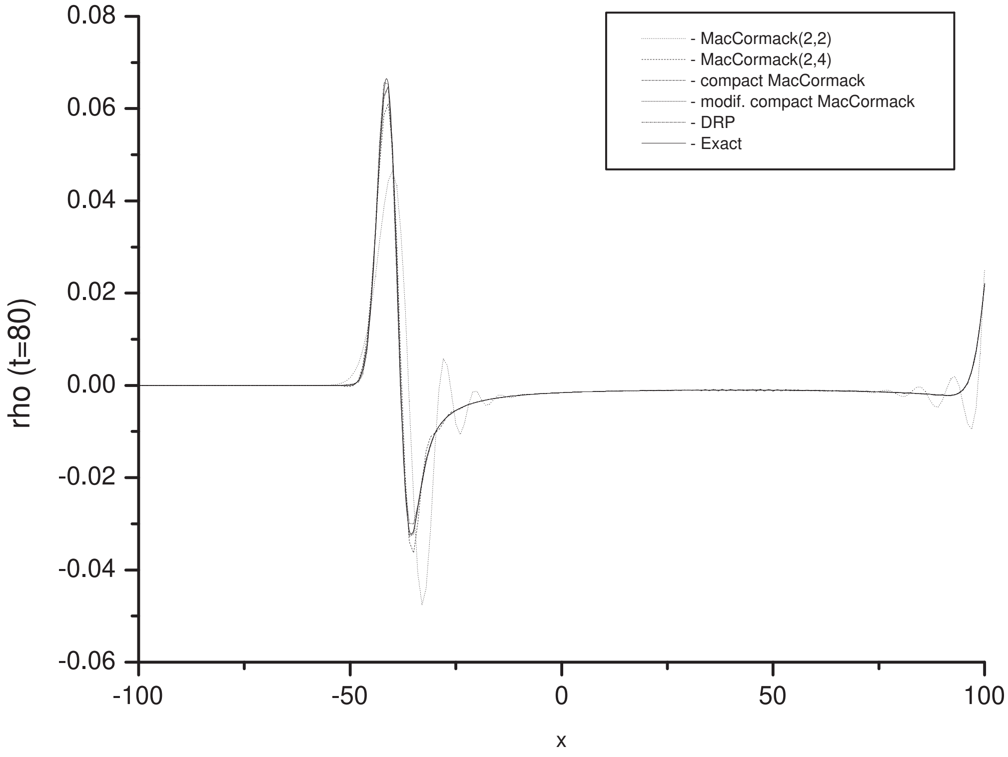

Figure 3: Density section (y=0, time 80)

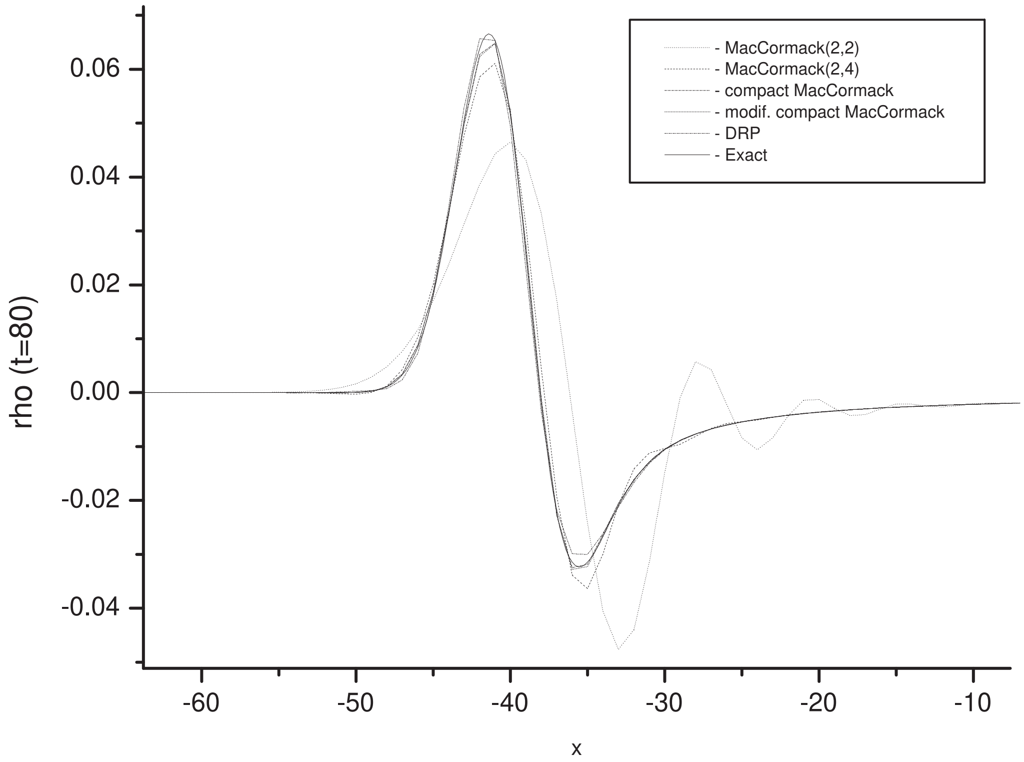

Figure 4: Density section (y=0, time 80, zoom)

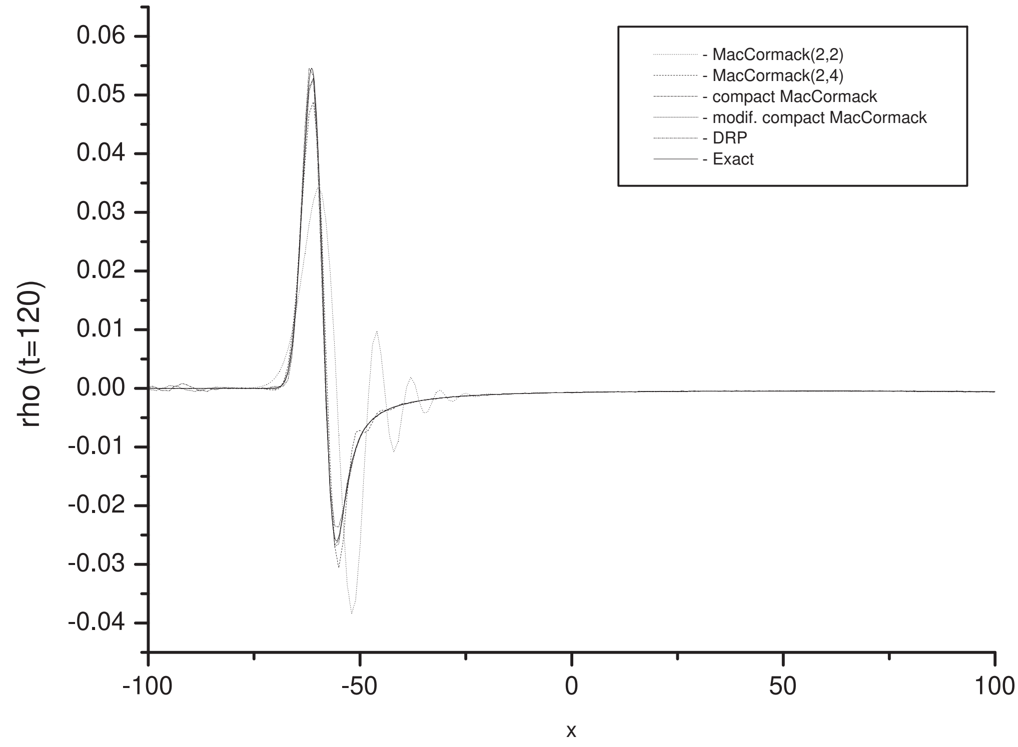

Figure 5: Density section (y=0, time 120)

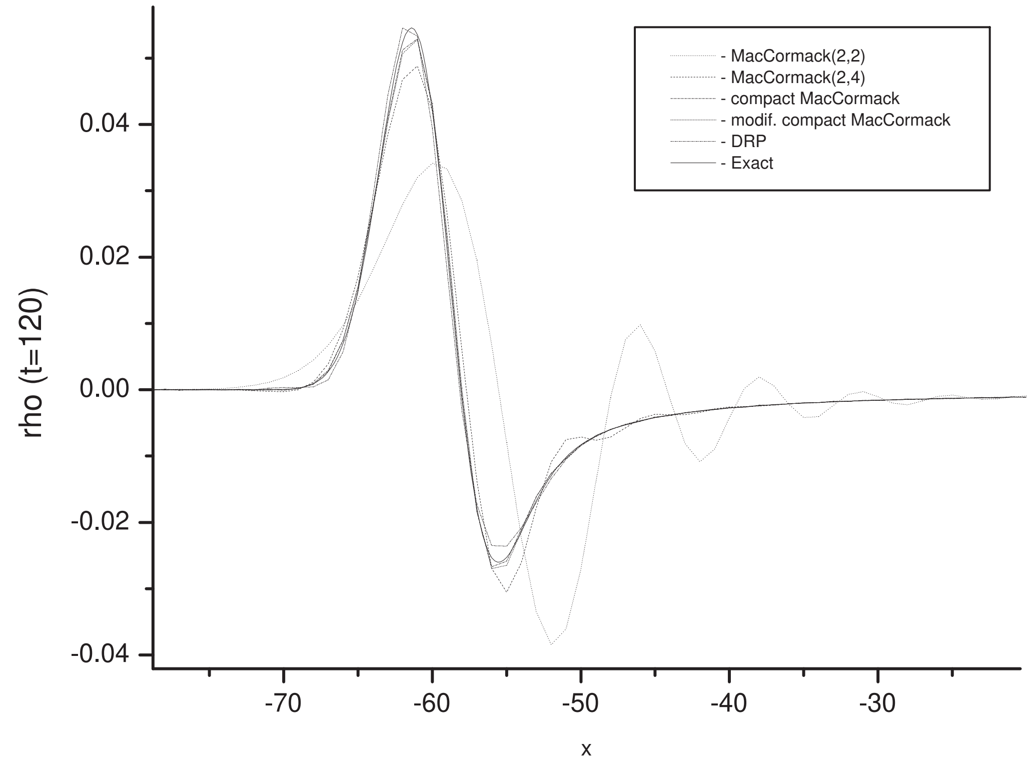

Figure 6: Density section (y=0, time 120, zoom)

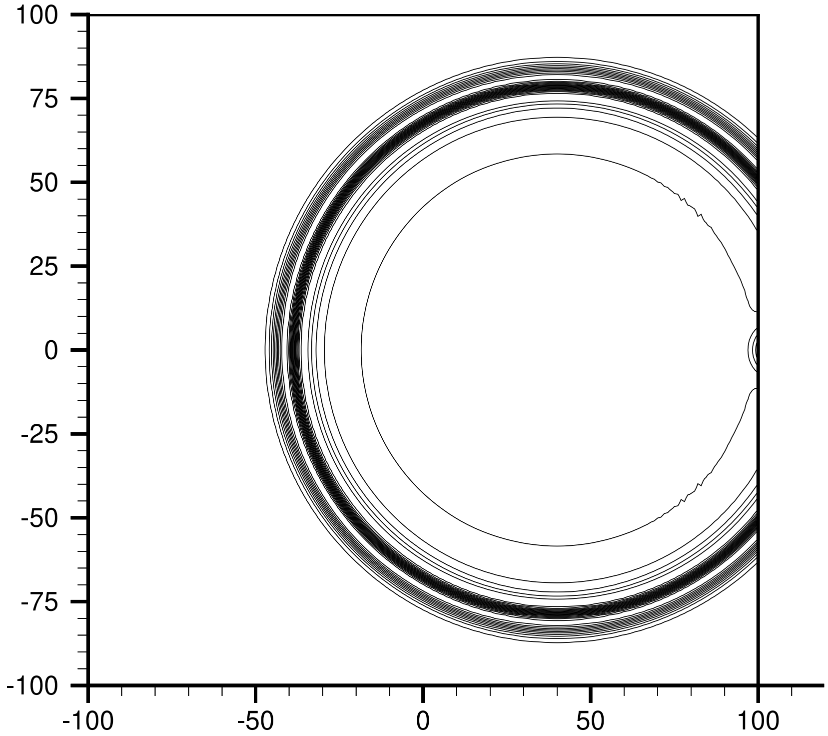

Figure 7: 2D-flow pattern calculated by compact Runge-Kutta scheme (TEST 1, time 80)

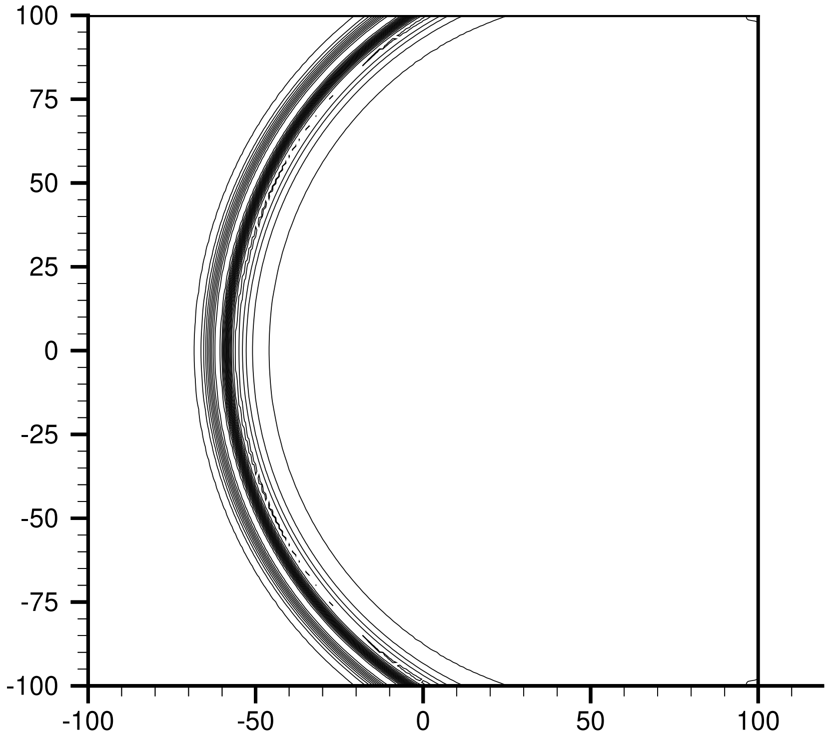

Figure 8: 2D-flow pattern calculated by compact Runge-Kutta scheme (TEST 1, time 120)

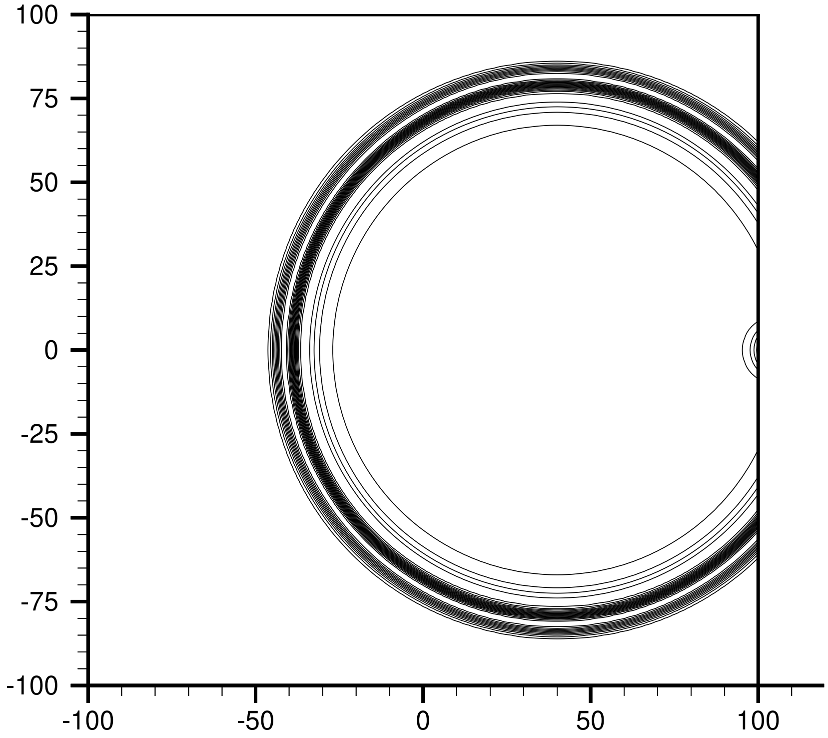

Figure 9: 2D-flow pattern calculated by DRP scheme (TEST 1, time 80)

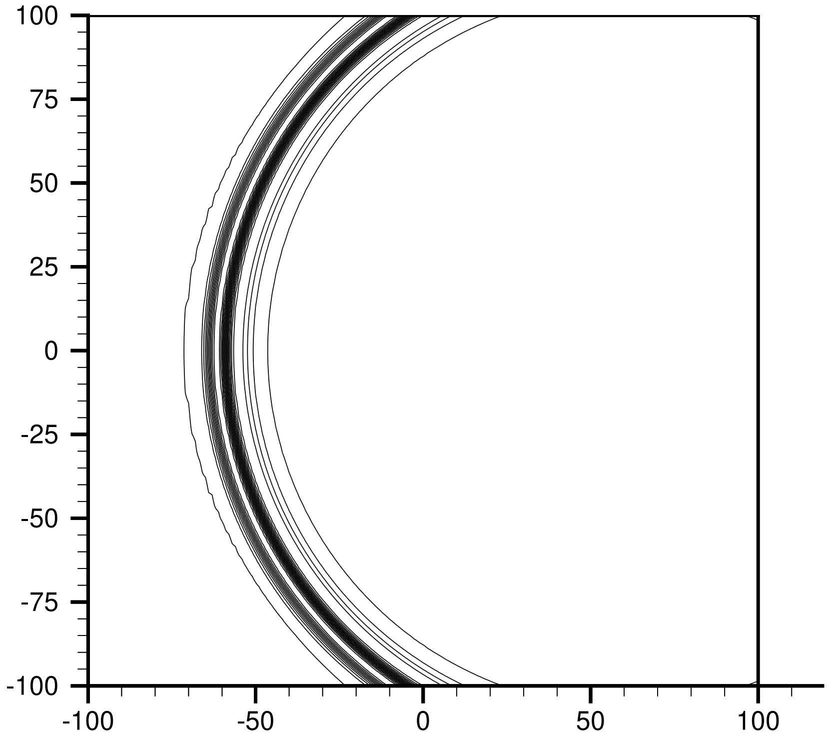

Figure 10: 2D-flow pattern calculated by DRP scheme (TEST 1, time 120)

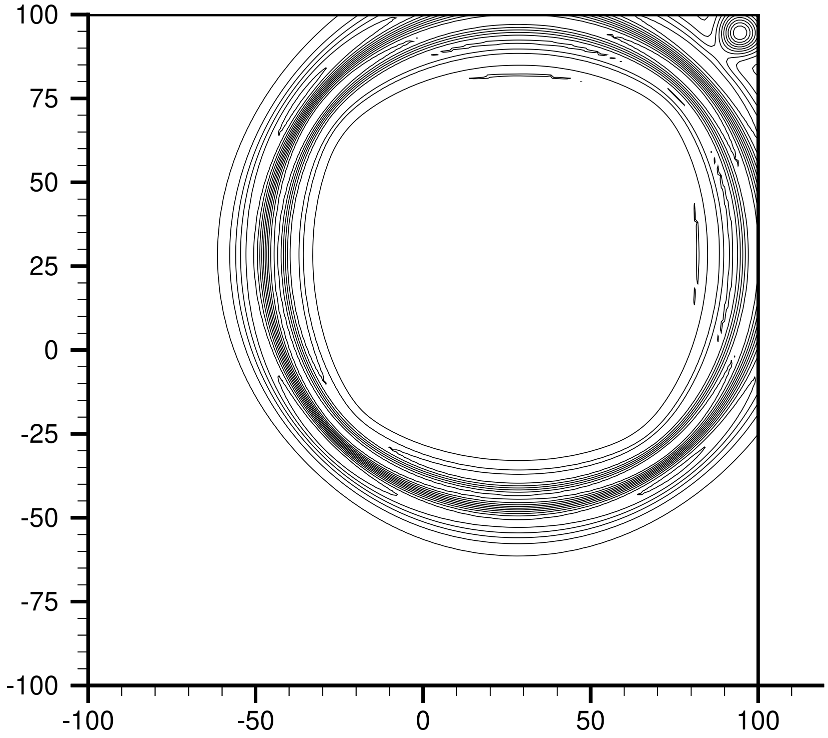

Figure 11: 2D-flow pattern calculated by MacCormack(2,2) scheme (TEST 2, time 80)

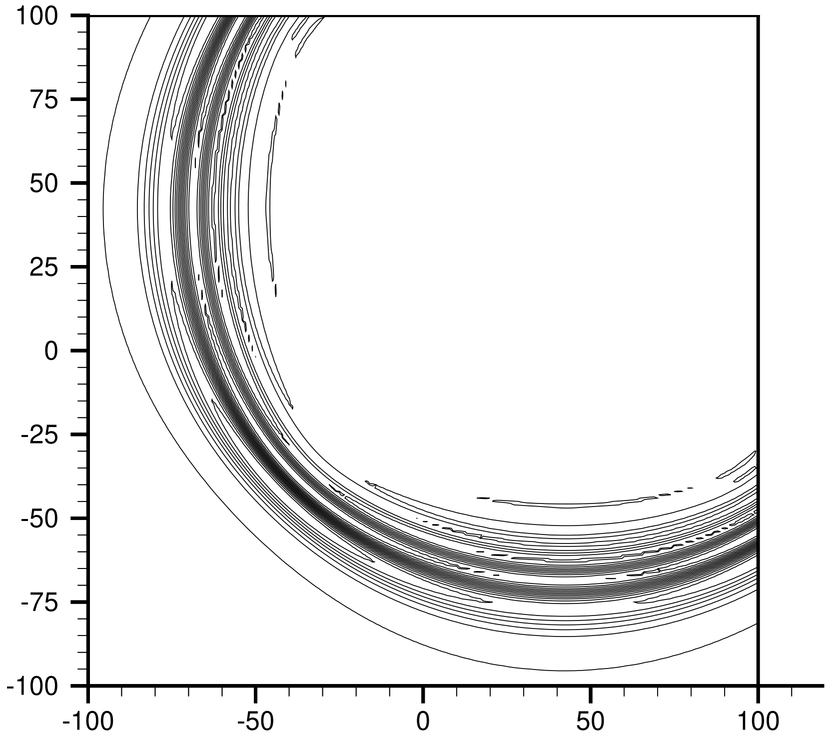

Figure 12: 2D-flow pattern calculated by MacCormack(2,2) scheme (TEST 2, time 120)

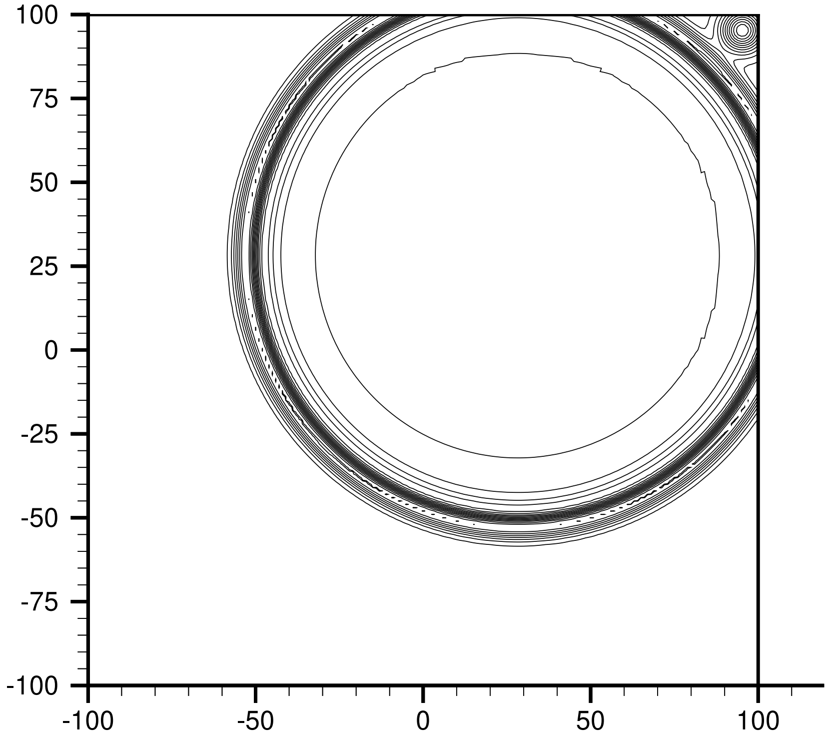

Figure 13: 2D-flow pattern calculated by compact Runge-Kutta scheme (TEST 2, time 80)

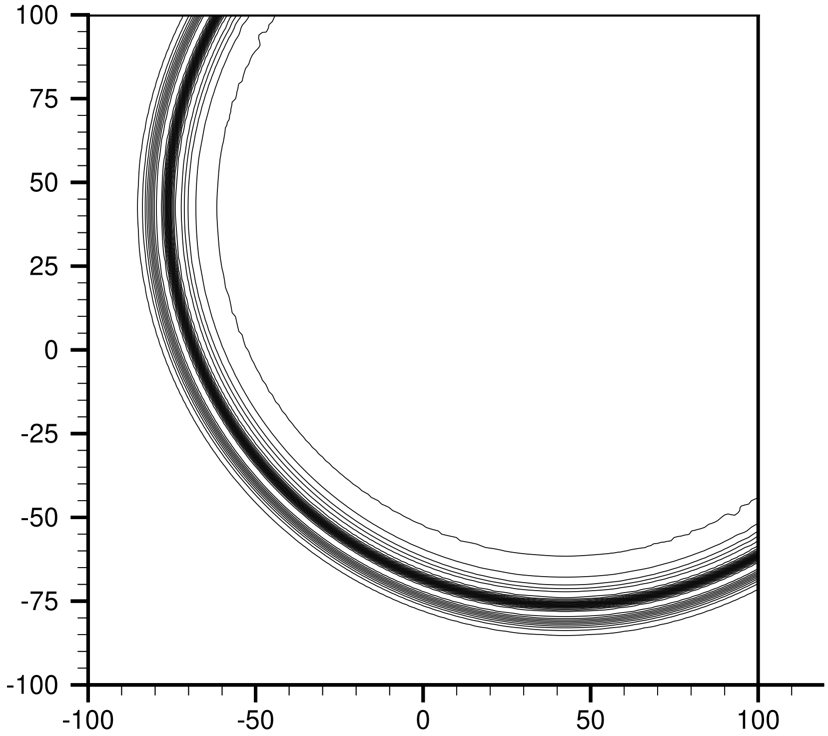

Figure 14: 2D-flow pattern calculated by compact Runge-Kutta scheme (TEST 2, time 120)

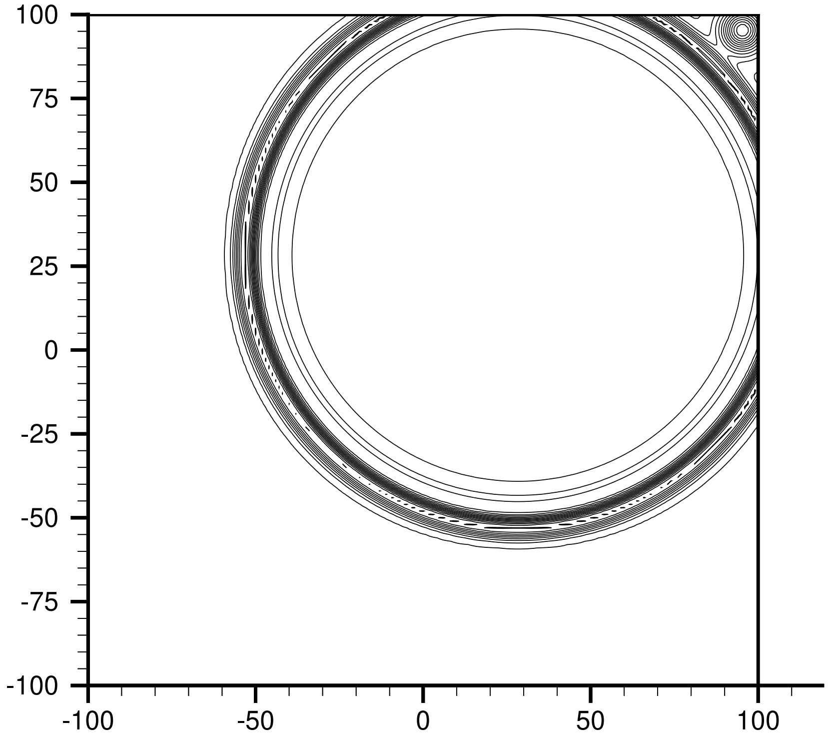

Figure 15: 2D-flow pattern calculated by DRP scheme (TEST 2, time 80)

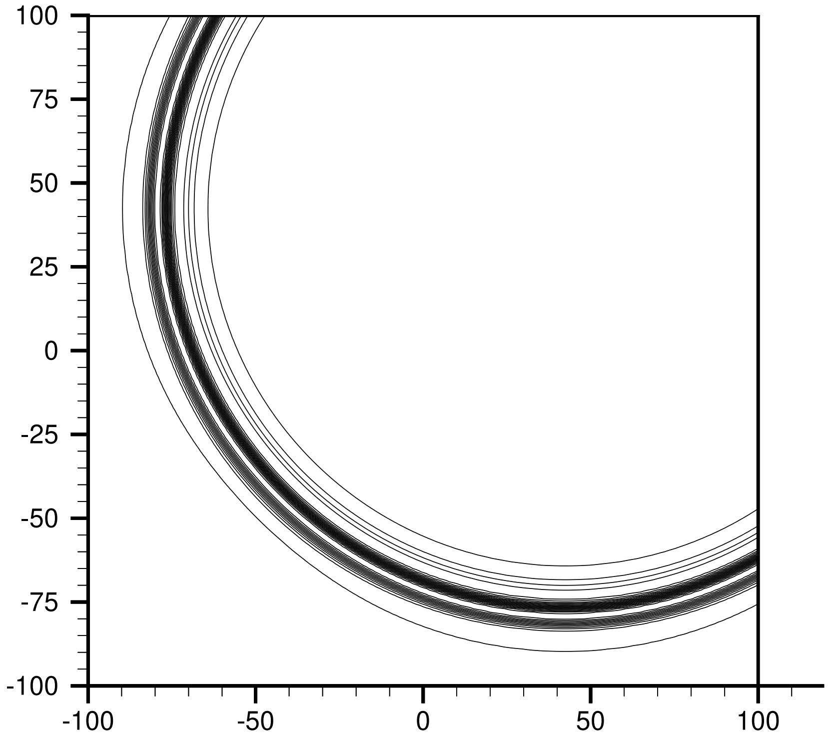

Figure 16: 2D-flow pattern calculated by DRP scheme (TEST 2, time 120)